Cavity design and optimization for organic microcavity OLEDs

J. Chan[1], Albert W. Lu[1], Chi Hang Cheung[2], Alan Man Ching Ng[2],
A. B. Djurišić[2], Yew Tong Yeow[1], A. D. Rakić[1]
[1] School of Information Technology and Electrical Engineering, The University of Queensland, Brisbane Qld4072, Australia
[2]Dept. of Physics, the University of Hong Kong, Pokfulam Road, Hong Kong

Abstract

We report on detailed simulations of the emission from microcavity OLEDs consisting of widely used organic materials, N,N′-di(naphthalene-1-yl)-N,N′-diphenylbenzidine (NPB) as a hole transport layer and tris (8-hydroxyquinoline) (Alq_3) as emitting and electron transporting layer. The thick silver film was considered as a top mirror, while silver or copper films on quartz substrate were considered as bottom mirrors. The electroluminescence emission spectra, electric field distribution inside the device, carrier density and recombination rate were calculated as a function of the position of the emission layer, i.e. interface between NPB and Alq_3. In order to achieve optimum emission from a microcavity OLED, it is necessary to align the position of the recombination region with the antinode of the standing wave inside the cavity. Once the optimum structure has been determined, the microcavity OLED devices were fabricated and characterized. The experimental results have been compared to the simulations and the influence of the emission region width and position on the performance of microcavity OLEDs was discussed.

Keywords: Microcavity OLEDs

1. INTRODUCTION

OLEDs has emerged as a potential candidate for application in display devices due to its prominent advantages in size, brightness and wide viewing angle [1, 2]. Since the development of first prototype of OLED by Tang and Van Slyke from Kodak, intense efforts have been seen in past decade on improving device performance thus leading to commercializing of small size OLED panels on market today [3]. In order to further improve and optimize this device for use in practical applications, device modeling of OLED characteristics is required to better understand the physical processes affecting the device performance. Device modeling has become a powerful tool as it avoids tedious experiments and offers exploration into wide range of critical microscopic behaviors which is not available via experiments. Work based on electrical and optical modeling have been documented separately in numerous studies, however, comprehensive device simulation that includes both electrical and optical models has been scarce [4, 5]. In this work, we aim to provide a detailed investigation into cavity design and thickness optimization of a bi-layer organic structure by examining both electrical and optical characteristics.

Electrons and holes are injected into organic layers from cathode and anode respectively, transported across organic layers and then recombined to form excitons. The excitons diffuse prior to undergoing radiative or non-radiative decay. As the optical thickness of the organic layers is of the order of a wavelength, standing wave pattern is observed. When the recombination zone is aligned with the anti-nodal region of the standing wave, enhancement in light output can be observed [6, 7]. Optimum recombination rate is obtained when balanced electron and hole injection and transport are achieved in the recombination region [8]. Furthermore, barrier to carrier injection and band offset in the organic layers are the dominant parameters that affect carrier transport behavior of the device [9]. To investigate the effects of those parameters, it is necessary to combine electrical and optical models together to examine the recombination mechanism in the OLED device so as to determine the most critical parameter associated with light generation.

In this work, the optimum thickness of organic layers is firstly determined from the resonant cavity model. Electrical carrier transport characteristics (electric field, carrier density and recombination region thickness) and optical properties (field distribution and emitted radiation spectrum) of a microcavity device are then simulated to determine the optimum structure. N,N′-di(naphthalene-1-yl)-N,N′-diphenylbenzidine (NPB) was used as hole transport layer and tris(8-

Photonics: Design, Technology, and Packaging II, edited by Derek Abbott, Yuri S. Kivshar, Halina H. Rubinsztein-Dunlop, Shanhui Fan, Proc. of SPIE Vol. 6038, 603824, (2006) · 0277-786X/06/$15 · doi: 10.1117/12.638368

hydroxyquinoline) aluminum (Alq_3) was used as a hole transport layer as well as an emissive layer. These organic layers are sandwiched between a silver (70nm) cathode and either silver or copper anode to provide different injection barrier for holes. Glass with 1 mm thickness was used as substrate. The model fully takes into account the optical dispersion in all the layers in the structure. The organic layer thickness values were chosen so that the position of the emission region was not too close to the metal cathode to avoid unrealistic model predictions since the model does not take into account exciton quenching due to defect states introduced during metal deposition. The calculated optical emission spectrum has been compared with the experimental results for Quartz/Ag/NPB/Alq_3/Ag device. The paper first describes the optical and electrical simulation models used including the simulation parameters and simulated experimental conditions. The outcome of simulation is then compared with the experimental data.

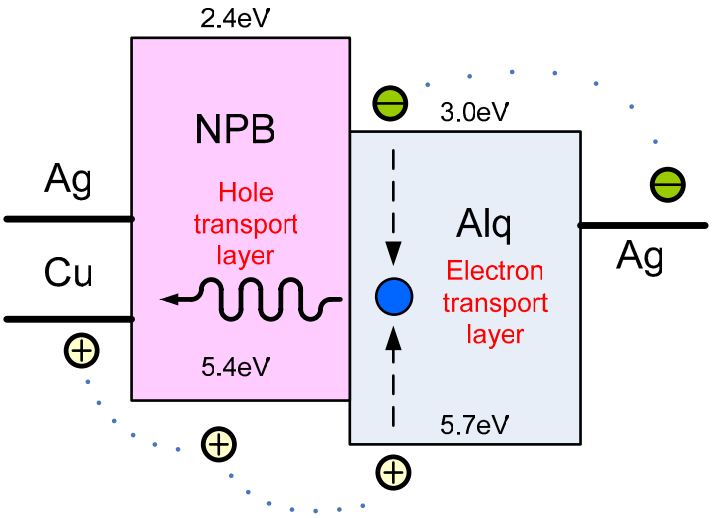

Figure 1: Typical OLED bi-layer device.

2. DESCRIPTION OF THE MODEL

2.1. Electrical model

Inside the organic semiconductor the electrical transport is modeled by the one-dimensional time-independent drift-diffusion model [9-11], which solves for a self-consistent solution of electron density, n, hole density, p and potential ψ using the semiconductor solver Atlas [12]. The model includes:

The continuity equation for n (electrons) and p (holes)

$$\begin{aligned} \frac{d}{dx}\left(-\mu_n n \frac{d\psi}{dx} + D_n \frac{dn}{dx}\right) &= R \\ \frac{d}{dx}\left(\mu_p p \frac{d\psi}{dx} + D_p \frac{dp}{dx}\right) &= R \end{aligned}, \qquad (1)$$

where μ_n and μ_p are the electron and hole mobilities and D_n and D_p are diffusion constants and R is the recombination rate. The μ and D are related by the well known Einstein relation. The carrier mobilities are modeled by the field-dependent form:

$$\begin{aligned} \mu_n(E) &= \mu_{n0} \exp\left[\sqrt{\frac{E}{E_0}}\right] \\ \mu_p(E) &= \mu_{p0} \exp\left[\sqrt{\frac{E}{E_o}}\right] \end{aligned}, \qquad (2)$$

where μ_{n0} and μ_{p0} are the zero field mobilities, E is the electric field and E_0 is the constant known as characteristic field. The recombination rate is taken to be optical only and modeled by the Langevin recombination coefficient γ [9, 10]:

$$R_{opt} = \gamma(pn - n_i^2)$$
$$\gamma = \frac{4\pi e \mu_R}{\varepsilon_r \varepsilon_0} \quad , \tag{3}$$

where n_i is the intrinsic concentration and μ_R is effective recombination mobility, taken to be the larger of the electron and hole mobilities in the material, $\varepsilon_r\varepsilon_0$ is the permittivity of the material. The effect of traps in the organic layers is not included in the current electrical model as the literature indicates the inclusion of traps has no significant effect on the simulation results obtained [9].

2.1.1. Poisson's equation

$$\frac{d^2\psi}{dx^2} = -\frac{e}{\varepsilon_r \varepsilon_o}[p(x) - n(x) + N_D - N_A], \tag{4}$$

where N_D and N_A are the ionized donor and acceptor dopant concentrations.

These equations are solved for the p-n junction structure using Schottky contact boundary conditions between a metal (which also serves as the reflecting surface for optical modeling) and the organic layer at the anode and the cathode. The barrier heights governing carrier injections are: ϕ_{bn} for electrons and ϕ_{bp} for holes and are related to the metal work function ϕ_m of the electrodes and the electron affinity of the organic material χ_c:

$$\phi_{bn} = (\phi_m - \chi_c)$$
$$\phi_{bp} = (E_g - \phi_{bn}) = E_g - (\phi_m - \chi_c) \quad . \tag{5}$$

The continuity equations and the Poisson equation are solved to obtain the carrier concentrations, electric field distributions and recombination rate. The thickness of recombination region can be determined from the recombination rate, which can be used to estimate the width of emission region (taking into account of exciton diffusion) to be included into the optical model.

2.1.2. Parameters used in simulation models

The material parameters used for modelling of carrier transport are obtained from literature [9-11]. The devices were simulated with forward bias of 5 volts. The mobility of majority carriers in the organic materials has been set to be two orders of magnitude higher than its minority carriers. Therefore NPB and Alq_3 are assumed to act as hole transport layer (HTL) and emission (EML) layer respectively. Where the simulation model requires a large number of material parameters only a few critical parameters including barrier heights to carrier injection, bandgaps of the organic materials and carrier concentrations have marked effects on the simulated result [9].

Parameters	**NPB**	**Alq_3**
Relative Permittivity	3.0	3.0
μ_{no} (cm^2/Vs)	$6.1\cdot10^{-6}$	$1.9\cdot10^{-6}$
μ_{po} (cm^2/Vs)	$6.1\cdot10^{-4}$	$1.9\cdot10^{-8}$
E_0 (V/cm)	$4.44\cdot10^{5}$	$7.1\cdot10^{4}$
N_c(cm^{-3})	$1\cdot10^{21}$	$1\cdot10^{21}$
N_v(cm^{-3})	$1\cdot10^{21}$	$1\cdot10^{21}$
N_A(cm^{-3})	$1\cdot10^{9}$	--
N_D(cm^{-3})	--	$1\cdot10^{9}$
E_g (eV)	3.0	2.7
χ_c (eV)	2.4	3.0
Parameters	**Ag**	**Cu**
ϕ_m (eV)	4.65	4.26

Table 1 Electrical simulation parameters

2.2. Optical model

The resonant modes of a microcavity have to satisfy the condition that the phase change during one round trip is a multiple of 2π. In other words, for normal incidence the following equation holds:

$$\sum_i \frac{4\pi}{\lambda} d_i n_i(\lambda) - \varphi_{top}(0,\lambda) - \varphi_{bot}(0,\lambda) = 2m\pi \quad , \tag{6}$$

where λ is the emission wavelength, $\varphi_{top}(\lambda)$, $\varphi_{bot}(\lambda)$ are the wavelength dependent phase changes upon reflection from top and bottom mirrors, respectively, m is an integer which defines the mode number, and the summation is performed over all the layers inside the cavity with thicknesses d_i and refractive indices $n_i(\lambda)$. The phase shift upon reflection from the mirrors is calculated using matrix method [13].

The intensity of the light output in the form of the electroluminescence (EL) spectrum was calculated using the method based on the equivalence between the probability of photon emission and the power radiated by a classical dipole antenna [14-19].

Consider the structure shown below.

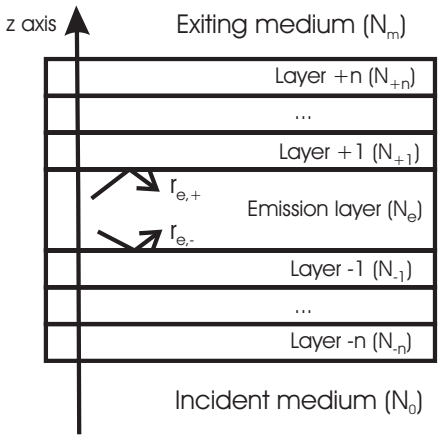

Figure 2: Microcavity multilayer structure

This cavity consists of two multilayer film DBR mirrors with a spacer layer sandwiched between them. In a layer with complex refractive index N_i, the amplitude of the wave vector is given by:

$$k_i = \frac{2\pi}{\lambda} N_i \quad , \tag{7}$$

where λ is the emission wavelength. The complex refractive index for each layer of the device was determined using Variable Angle Spectroscopic Ellipsometry (VASE). The complex refractive index is then determined from Ellipsometry data by using the Lorentz-Drude model [20-24]. Lorentz-Drude model parameter extraction was performed by using simulated annealing algorithm.

When considering wave propagation through thin film layers, it is convenient to resolve the wave vector into two components: the component normal to the direction of propagation and the component along the direction of propagation (we use the z-axis as the axis of propagation), which is given by:

$$\kappa = k_i \sin(\alpha_i), \tag{8}$$

and

$$k_{z,i} = k_i \cos(\alpha_i) = \sqrt{k_i^2 - \kappa^2} \quad , \tag{9}$$

respectively, where α_i is the angle the wave makes with the z-axis.

The total power F emitted by a dipole antenna located within the multilayer structure normalized to the power output of the same dipole in an infinite medium is given by:

$$F = \int_0^\infty K(\kappa) d\kappa^2 \quad , \tag{10}$$

where K is the power density per unit $d\kappa^2$.

The power density (K) can be resolved into the TM and TE component, with each component separated into power densities for dipoles oriented parallel and perpendicular to the z-axis. With this in mind, the power densities can be defined as:

$$K_{\perp}^{TM} = \frac{3}{4} \Re \left[\frac{\kappa^2}{k_e^2 k_{z,e}} \frac{\left(1 - a_+^{TM}\right)\left(1 - a_-^{TM}\right)}{1 - a^{TM}} \right], \tag{11}$$

$$K_{\perp}^{TE} = 0, \tag{13}$$

$$K_{\parallel}^{TM} = \frac{3}{8} \Re \left[\frac{k_{z,e}}{k_e^3} \frac{\left(1 + a_+^{TM}\right)\left(1 + a_-^{TM}\right)}{1 - a^{TM}} \right], \tag{14}$$

$$K_{\parallel}^{TE} = \frac{3}{8} \Re \left[\frac{1}{k_e k_{z,e}} \frac{\left(1 + a_+^{TE}\right)\left(1 + a_-^{TE}\right)}{1 - a^{TE}} \right], \tag{15}$$

where e denotes the emissive layer (sandwiched between top and bottom mirrors) and a is the reflection coefficient of the mirror with respect to the location of the dipole, defined as:

$$a_{+/-}^{TM/TE} = r_{e,+/-}^{TM/TE} \exp\left(-2jk_{z,e} z_{+/-}\right) \quad , \tag{16}$$

$$a^{TM/TE} = a_+^{TM/TE} a_-^{TM/TE} \quad , \tag{17}$$

where z_+ is the dipoles' distance from the top mirror, z_- is the dipoles' distance from the bottom mirror and r is the amplitude reflection coefficient of the top and bottom mirrors calculated using the modified transfer matrix approach of Katsidis and Siapkas [23, 24].

For randomly oriented dipole antenna (equal probability for all orientation direction), the power density is given by:

$$K^{TM,TE} = \frac{1}{3} K_{\perp}^{TM,TE} + \frac{2}{3} K_{\parallel}^{TM,TE} . \quad (18)$$

The overall power density will then be the average of the TM and TE component.

3. EXPERIMENTAL DETAILS

The materials used (Alq_3 and NPB from H. W. Sands Corp.) were purified by vacuum sublimation before fabrication. Devices were fabricated by vacuum deposition. The pressure during evaporation was of the order 10^{-4} Pa. The evaporation rate was kept at ~1 Å/s. The distance from source to film was about 23 cm to ensure uniformity of film thickness, and the substrate holder was rotating. The thickness of the films was controlled by a quartz thickness monitor. The electrodes consisted of Cu and Ag films of various thickness. The electroluminescence (EL) spectra were measured using Control Development fiber optic spectrometer (PDA 512 USB), while luminance-current-voltage (L-I-V) characteristics were measured in ambient environment using a Keithley 2400 sourcemeter and luminance meter (Minolta LS-100).

4. RESULTS AND DISCUSSION

Optimum thickness of the cavity is determined to be approximately 260 nm with cavity order of one. The electric field intensity distribution was then calculated for the device in order to align the antinode of the field with the light emission region of the device (see Fig. 3). Two devices were simulated, one with thickness of NPB and Alq_3 to be 210 and 50 (210/50) respectively, where the second antinode of the device was aligned with the emission region. On the other hand, the thickness of the second device was determined to be 50/210 so that the emission region of the device is aligned with the first antinode of the optical field distribution.

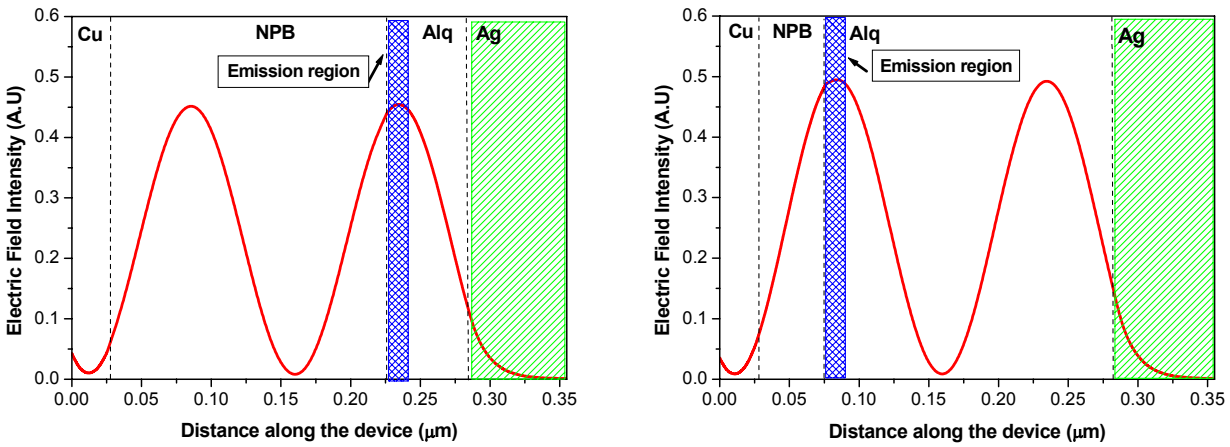

Figure 3: Simulated electric field intensity of device with different NPB/Alq_3 thickness

After the thickness of the device was determined, the electrical properties for 210/50 device were simulated as shown in Fig. 4. When a forward bias voltage of 5 V was applied, holes were injected from anode into NPB layer and accumulated near the NPB/Alq_3 interface due to offsets in the HOMO bands. Alq_3 layer acted as a hole blocking layer in this case. On the other hand, amount of electrons in the Alq_3 layer is negligible at steady state since most of electrons have already formed excitons. Accumulation of holes in the NPB/Alq_3 interface caused electric field in Alq_3 region to be higher than that of NPB layer according to Poisson's equation.

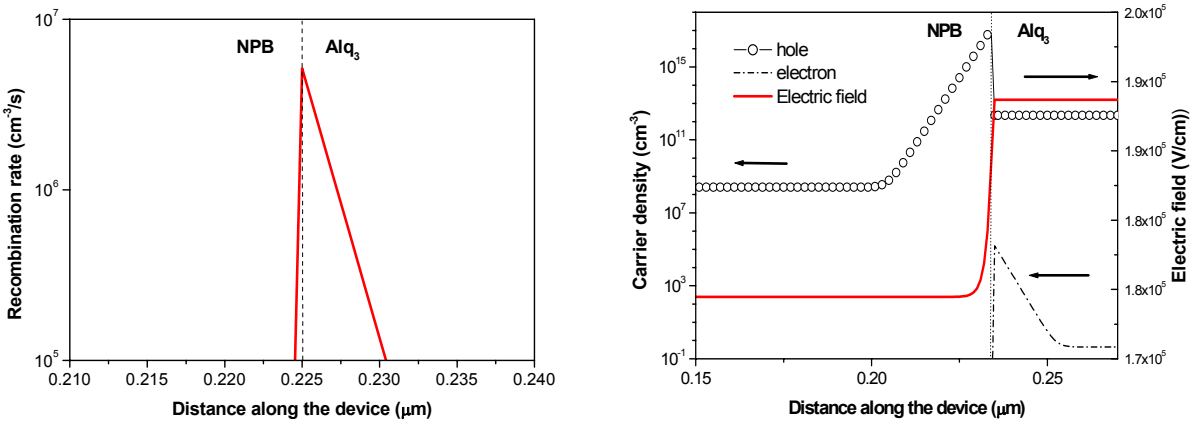

Figure 4: a) Simulated recombination rate (left) and b) simulated carrier density and electric field (right) for the 210/50 device.

Figure 4a) shows the simulated carrier recombination rate in the same device. It is clearly observed that majority of the recombination occurred within 5 nm from the NPB/Alq_3 interface in the Alq_3 layer. The result corresponds to Tang's finding which reported that in an Alq_3-based bi-layer structure, recombination zone generally occurs within 5 nm from the HTL/EML interface and emission zone usually extends to 20 nm due to exciton diffusion [25].

When the anode of the device is formed by Ag film, the hole injection barrier changes from 0.75 to 1.14 eV and it has significantly reduced the amount of holes injected into the NPB layer. The barrier offset in the NPB/Alq_3 interface caused holes to pile up as before. This decreased the recombination rate by two orders of magnitude compared to the previous device. The effect on the lowered recombination rate also reflected on the electro-luminance (EL). The EL of the device with Ag anode is significantly lowered when compared to device with Cu anode. On the other hand, if the electron injection barrier is further increased, negligible number of electrons will be injected into the Alq_3 layer, thus leading to negligible recombination rate. Therefore, in order to obtain better recombination efficiency, balanced injection of carriers into the emission region is essential.

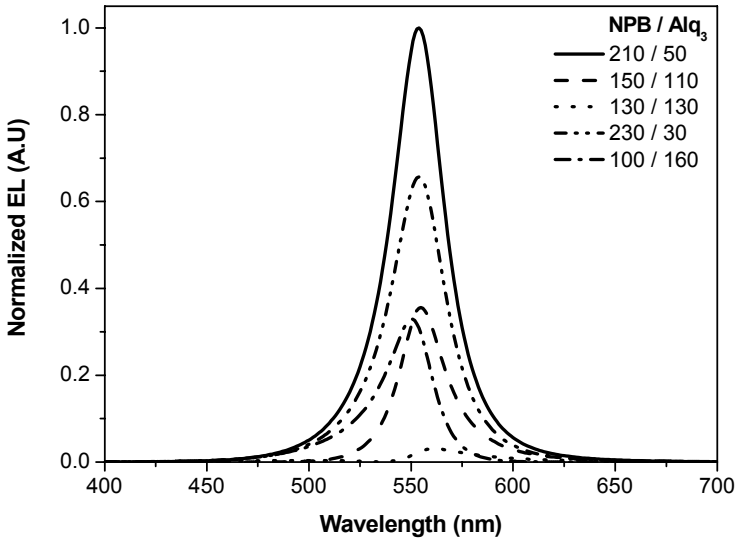

Figure 5: Normalized EL comparisons for 5 devices with varying relative layer thicknesses.

Figure 5 shows simulated electroluminescence (EL) spectrum for five devices with varying NPB/Alq_3 interface position, while maintaining cavity thickness at 260 nm. Ag is used as both anode and cathode. It can be observed that the EL intensity is the strongest for the 210/50 device with recombination region aligned with the antinode of the field. The luminance spectrum was simulated with the emission layer thickness of 20 nm based on the recombination region thickness of 5 nm obtained from the electrical simulation. Finally, Ag/NPB(210)/Alq_3(50)/Ag bi-layer device is fabricated and its electroluminescence at varying angle was measured and compared with the optical model. The simulation model predicts properly the blue-shift of EL peak with increasing angle and matches the main features of experimental results reasonably well.

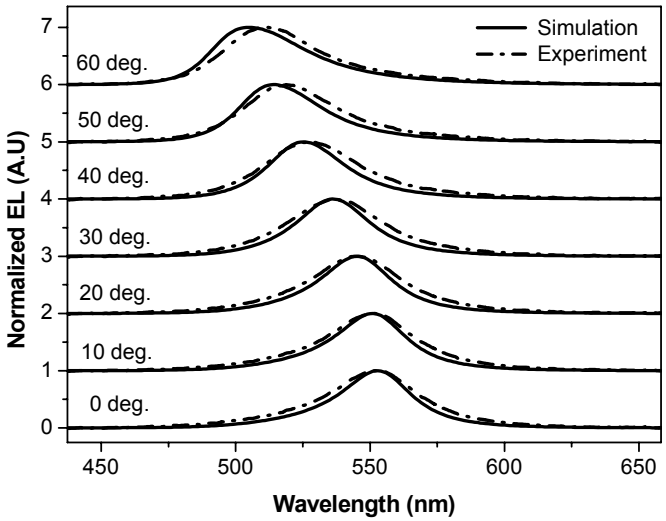

Figure 6: Comparison between the experimental and simulated EL spectrum.

5. CONCLUSION

We have simulated both electrical and optical behavior of bi-layer OLEDs by use of numerical and analytical models. The recombination width obtained from the electrical model was found to be within 5 nm from the NPB/Alq_3 interface and located in the Alq_3 region, which corresponds to the experimentally observed values. The calculated recombination region width combined with the diffusion length was used to determine the emission layer thickness that was used in the optical simulation model. In order to achieve better recombination efficiency, balanced carrier transport to the emissive layer is essential. By simulating the device with different choice of anode material, we have observed that injection barrier for electrons and holes is the major parameter that affects the carrier transport in the device. By aligning the position of the antinode of optical field intensity within the device with the electrical recombination region, enhancement in the overall light output of the device was achieved. Good agreement between the simulated and experimental electro-luminance spectra was observed.

REFERENCE

[1] W. Brutting, S. Berleb, and A. G. Muckl, "Device physics of organic light-emitting diodes based on molecular materials," *Organic Electronics: physics, materials, applications*, vol. 2, pp. 1-36, 2001.

[2] L. S. Hung and C. H. Chen, "Recent progress of molecular organic electroluminescent materials and devices," *Materials Science and Engineering R: Reports*, vol. 39, pp. 80, 2002.

[3] C. W. Tang and S. A. VanSlyke, "Organic electroluminescent diodes," *Applied Physics Letters*, vol. 51, pp. 913-15, 1987.

[4] B. Ruhstaller, T. Beierlein, H. Riel, S. Karg, J. C. Scott, and W. Riess, "Simulating Electronic and Optical Processes in Multilayer Organic Light-Emitting Devices," *IEEE Journal on Selected Topics in Quantum Electronics*, vol. 9, pp. 723-731, 2003.

[5] C.-C. Lee, M.-Y. Chang, Y.-D. Jong, T.-W. Huang, C.-S. Chu, and Y. Chang, "Numerical simulation of electrical and optical characteristics of multilayer organic light-emitting devices," *Japanese Journal of Applied Physics, Part 1: Regular Papers and Short Notes and Review Papers*, vol. 43, pp. 7560-7565, 2004.

[6] S. K. So, W. K. Choi, L. M. Leung, and K. Neyts, "Interference effects in bilayer organic light-emitting diodes," *Applied Physics Letters*, vol. 74, pp. 1939-1941, 1999.

[7] S. Dirr, A. Bohler, S. Wiese, H.-H. Johannes, and W. Kowalsky, "Organic light emitting diodes with reduced spectral and spacial halfwidths," *Japanese Journal of Applied Physics, Part 1 (Regular Papers, Short Notes & Review Papers) Solid State Devices and Materials, 16-19 Sept. 1997*, vol. 37, pp. 1457-61, 1998.

[8] A. B. Walker, A. Kambili, and S. J. Martin, "Electrical transport modelling in organic electroluminescent devices," *Journal of Physics: Condensed Matter*, vol. 14, pp. 9825-76, 2002.

[9] S. J. Martin, G. L. B. Verschoor, M. A. Webster, and A. B. Walker, "The internal electric field distribution in bilayer organic light emitting diodes," *Organic Electronics*, vol. 3, pp. 129-41, 2002.

[10] M. A. Webster, J. Auld, S. J. Martin, and A. B. Walker, "Simulation of the external quantum efficiency for bilayer organic light emitting devices," presented at Organic Light-Emitting Materials and Devices VII, Aug 4-6 2003, San Diego, CA, United States, 2004.

[11] C. D. J. Blades and A. B. Walker, "Simulation of organic light-emitting diodes," *Synthetic Metals 2nd International Conference on Electroluminescence of Molecular Materials and Related Phenomena (ICEL-2), May 15-May 18 1999*, vol. 111, pp. 335-340, 2000.

[12] Silvaco, *ATLAS User Manual*, vol. 1. Santa Clara: Silvaco International, 2000.

[13] A. H. Macleod, *Thin-film optical filters*: Institute of Physics Publishing, 2000.

[14] K. Neyts, P. De Visschere, D. K. Fork, and G. B. Anderson, "Semitransparent metal or distributed Bragg reflector for wide-viewing-angle organic light-emitting-diode microcavities," *Journal of the Optical Society of America B (Optical Physics)*, vol. 17, pp. 114-19, 2000.

[15] K. A. Neyts, "Simulation of light emission from thin-film microcavities," *Journal of the Optical Society of America A: Optics and Image Science, and Vision*, vol. 15, pp. 962, 1998.

[16] W. Lukosz, "Theory of optical-environment-dependent spontaneous-emission rates for emitters in thin layers," *Physical Review B (Condensed Matter)*, vol. 22, pp. 3030-8, 1980.

[17] W. Lukosz, "Light emission by multipole sources in thin layers. I. Radiation patterns of electric and magnetic dipoles," *Journal of the Optical Society of America*, vol. 71, pp. 744-54, 1981.

[18] W. Lukosz and R. E. Kunz, "Light emission by magnetic and electric dipoles close to a plane interface. I. Total radiated power," *Journal of the Optical Society of America*, vol. 67, pp. 1607-15, 1977.

[19] W. Lukosz and R. E. Kunz, "Light emission by magnetic and electric dipoles close to a plane dielectric interface. II. Radiation patterns of perpendicular oriented dipoles," *Journal of the Optical Society of America*, vol. 67, pp. 1615-19, 1977.

[20] A. D. Rakic, A. B. Djurisic, J. M. Elazar, and M. L. Majewski, "Optical properties of metallic films for vertical-cavity optoelectronic devices," *Applied Optics*, vol. 37, pp. 5271-83, 1998.

[21] A. B. Djurisic, J. M. Elazar, and A. D. Rakic, "Modeling the optical constants of solids using genetic algorithms with parameter space size adjustment," *Optics Communications*, vol. 134, pp. 407-414, 1997.

[22] A. B. Djurisic, A. D. Rakic, and J. M. Elazar, "Modeling the optical constants of solids using acceptance-probability-controlled simulated annealing with an adaptive move generation procedure," *Physical Review E (Statistical Physics, Plasmas, Fluids, and Related Interdisciplinary Topics)*, vol. 55, pp. 4797-803, 1997.

[23] C. C. Katsidis and D. I. Siapkas, "General transfer-matrix method for optical multilayer systems with coherent, partially coherent, and incoherent interference," *Applied Optics*, vol. 41, pp. 3978-87, 2002.

[24] C. L. Mitsas and D. I. Siapkas, "Generalized matrix method for analysis of coherent and incoherent reflectance and transmittance of multilayer structures with rough surfaces, interfaces, and finite substrates," *Applied Optics*, vol. 34, pp. 1678-83, 1995.

[25] C. W. Tang, S. A. VanSlyke, and C. H. Chen, "Electroluminescence of doped organic thin films," *Journal of Applied Physics*, vol. 65, pp. 3610-16, 1989.